IEEE Access
Multidisciplinary | Rapid Review | Open Access Journal

Received April 1, 2019, accepted May 6, 2019, date of publication May 29, 2019, date of current version November 4, 2019.

Digital Object Identifier 10.1109/ACCESS.2019.2919784

Incoherent Space Beam Combining of Fiber-Transmitted Semiconductor Lasers for Oil Well Laser Perforation

YANG BAI[1,2], GUANGZHI LEI[3], HAOWEI CHEN[1,2], XIAOQIANG FENG[1,2], DIAO LI[1,2], AND JINTAO BAI[1,2]

[1]State Key Laboratory Incubation Base of Photoelectric Technology and Functional Materials, National Photoelectric Technology, and Functional Material sand Application of Science and Technology International Cooperation Center, Institute of Photonics &Photon-Technology, Northwest University, Xi'an 710069, China
[2]Shaanxi Engineering Technology Research Center for Solid State Lasers and Application, Northwest University, Xi'an 710069, China
[3]Space Optical Technology Research Department, Xi'an Institute of Optics and Precision Mechanics of CAS, Xi'an 710119, China

Corresponding author: Jintao Bai (baijt@nwu.edu.cn)

This work was supported by the National Key Research and Development Plan of China under Grant 2017YFB0405102.

ABSTRACT This paper demonstrates a 19 × 1 incoherent space beam combiner tailored for oil well laser perforation, which is used for an incoherent laser beam combining of 19 fiber-transmitted semiconductor lasers around a wavelength of 972 nm. The parameters of the combiner and its used optical lens are optimized, which is attributed to the theoretical analysis of the variation law between the radii, the spacing of collimating laser beams, and the spot overlap rate of the combined laser beam, respectively, and the simulation of the cross-sectional energy distribution of the beam combiner. A beam combining the power of 10.159 kW is achieved with an average beam combining efficiency of higher than 98.2%, a beam combining length of 300 mm, and a focal spot diameter of 21 mm. A laser perforation experiment is performed for a granite sample using a 10-kW space incoherent beam laser, and a perforation depth of 960 mm is obtained. This paper underscores the design philosophy of the incoherent space beam combiner with ultra-high laser power, a long beam combining length, a simple structure, and a high downhole transmission safety, and builds the foundation for applications of the incoherent space beam combined laser in the oil well perforation.

INDEX TERMS Fiber-transmitted, incoherent space beam combining, laser perforation, overlapping efficiency, 10 kW.

I. INTRODUCTION

High power (>10 kW) laser perforation has become a hotspot in oil well exploration and development since the advantages of high porosity and permeability, free debris, short completion time and low cost [1]–[7]. Fiber transmission is an effective method to reduce the loss of high power laser in oil wells. However, due to limitations such as nonlinear effects, fiber surface damage, thermal lens effect, and single-mode fiber attenuation etc., the output power of all-fiber lasers cannot be increased infinitely. In particular, a single fiber is difficult to adapt to the harsh downhole environment of high temperature, high pressure and high corrosion, which brings high safety risks to the transmission of the high-power laser in oil wells [8]–[10]. Incoherent beam combining by using multiple fiber-transmitted laser beams is an effective method to reduce the transmission risk of high power laser in a single fiber and improve the output power of the laser. Currently, mainstream high power incoherent beam combining technologies including all-fiber beam combining using all-fiber beam combiner [11]–[13], spectral beam combining using diffraction grating and polarization beam splitter [14]–[16], and space beam combining using mutually parallel groups of optical collimating lens and individually controlled steering mirrors [17]–[20]. Using these techniques, the power of CW laser with incoherently combined beams has exceeded 10 kW [11], [14], [17]. However, all-fiber beam combiner is fabricated via fiber melting and splicing processes [11], [21]. People can neither quickly replaces the fiber laser simply with plug-and-play manner, nor repair the combiner quickly on site. In diffraction grating and polarization beam splitter, grating-based devices are

The associate editor coordinating the review of this manuscript and approving it for publication was Bora Onat.

sensitive to position and beam quality for narrow spectral line-width (∼GHz) and small beam size (∼1 mm) [22], [23]. The factors lead to extremely complicated manufacturing processes of diffraction gratings and polarization beam splitters for the 10 kW-level laser incoherent beam combining.

The space beam combiner has a number of advantages over other beam combiners, such as simple manufacturing process, high combining efficiency, high structural strength, easy maintenance, long service life, excellent environmental adaptability. Therefore, it has been widely used in high-energy laser weapon systems [22]–[24]. However, the use of multiple independently controlled steering mirrors results in a larger optical aperture of the conventional space beam combiner (300-600 mm). And it is difficult to increase the number of laser beams participating in the space beam combining without increasing the optical aperture (mostly 2-6 laser beams). Thus, it is difficult for the conventional space beam combiners to be placed in most oil wells with a diameter smaller than 200 mm [25], [26]. Transmission power and risks of the laser beam in a single fiber also increase due to the small number of laser beams in the space beam combining.

In this paper, we demonstrate a 19 × 1 incoherent space beam combiner (ISBC) with a set of optical lenses based on the characteristics of high power laser required by oil well laser perforation. The parameters of the combiner and its used optical lens are optimized, which is attributed to the theoretical analysis of the variation law between the radii, spacing of collimating laser beams and the spot overlap rate of combined laser beam respectively, and the simulation of the cross section energy distribution of the beam combiner. The combiner has a 130-mm external diameter consisting of 19 identical beam collimating units (BCUs) and a common space beam combining unit (SBCU), and it connects to 19 independently fiber-transmitted semiconductor lasers around a wavelength of 972 nm and output power of 550 W. Nineteen BCUs are arranged according to the ''center + inner, outer concentric circles'' coaxial scheme, that is, the intersections of the 12 BCUs' optical axes and the vertical plane of the laser beam form an outer circle. The intersection of the 6 BCUs' optical axes and the same incident surface form an inner circle. The centers of the two circles are overlapped. The intersection of the optical axis of the nineteenth BCU and the same incident surface locate at the center of the circle. By this ''geometric'' beam coupling scheme, a single laser beam with a CW beam combining power more than 10 kW and a beam combining length of 300 mm are obtained. In addition, as a feasibility study, a laser perforation experiment with a penetration depth of 960 mm for a granite sample is performed using a 10 kW incoherent space beam combined laser. To the best of our knowledge, this is the first report of laser perforation for rock samples using an incoherent space beam combined laser, which shows the feasibility and potential of oil well laser perforation based on incoherent space beam combining.

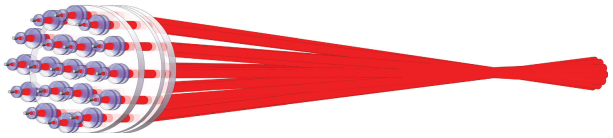

FIGURE 1. Optical schematic of 19 × 1 incoherent space beam combining.

II. DESIGN AND SIMULATION OF THE COMBINER

The optical design principle of the 19 × 1 ISBC is shown in Fig. 1. This space beam combiner consists of 19 identical BCUs and one SBCU. The optical axes of all optical elements were paralleled. The 19 BCUs are arranged according to the ''center + inner, outer concentric circles'' coaxial scheme. The 19 diverging 972-nm laser beams simultaneously propagate from the fibers to 19 BCUs and change into 19 paralleled collimated laser beams. The function of the SBCU was to combine 19 parallel collimated laser beams in the space based on the optical convergence and obtain a single laser beam with a longer beam combining length. The energy distribution of 19 parallel laser beams in the longer beam combination length is overlapping rather than discretely distributed, which ensures that a longer laser perforation depth is obtained. The maximum CW output power of each 972-nm laser was higher than 550 W. The transmission fibers are in multimode with SMA905 connectors. The sectional diameter of the SMA905 connector was 8 mm. The diameter (M_d) and numerical aperture ($N.A.$) of each multimode transmission fiber were 440 μm and 0.22 (i.e., equivalent to a divergence full-angle $\theta_o = 2 \times \arcsin(0.22)$, respectively).

In the beam combining, an overlapping efficiency of 85% is usually used as a critical value to evaluate the quality of the combined beam, and the distance between two points with an overlapping efficiency equals to 85% is defined as the beam combining length along the laser propagation direction. Therefore, our incoherent space beam combining using 19 collimated laser beams generally have an overlapping efficiency of more than 85% over a longer beam combining length, which is a key factor to be considered in the design of the combiner.

In this work, the calculation formula of the overlapping efficiency of laser beam combining was deduced, as shown in the following. The parameter selection and beam combining precision of the space beam combiner were evaluated by using this formula. The arrangement of the 19 collimated beam spots on the incident surface of the SBCU is shown in Fig. 2(a). And Fig. 2(b) shows the positional relationship of the central beam spot and any other beam spot on this incident surface and the positional relationship of these two spots after transmitting a certain distance (l, it was set from 0 to two times of the combined focal length). The r_0 and r_i ($r_0 = r_i$) are the spot radii of the collimated center beam spot and any other collimated beam spot ($i = 1, 2, 3...18$) on the incident surface of the SBCU, respectively. It should be noted that besides the collimated beam at the center, the other 18 collimated beams are elliptical on the reference plane

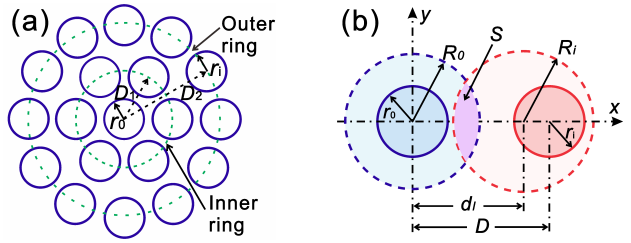

FIGURE 2. (a) Arrangement in concentric circles of the 19 collimated beam spots on the incident surface of the SBCU. (b) The positional relationship between the central beam spot and any other beam spot on the incident surface of the SBCU and the vertical plane after a certain transmitting distance *l*.

perpendicular to the normal of the SBCU. The area calculation formula for the ellipse is $S_e = \pi a_e b_e$, where $a_e = R_i$, $b_e = R_i \cos\phi$, $\cos\phi = D/F$. D and F are the beam separation distance on the incident surface and combined focal length of the SBCU, respectively. However, the value of D (a few centimeter) is very small compared to the value of F (> 1 m). The area difference between the ellipse ($S_e = \pi R_i^2 \cos\phi$) and the circle ($S_c = \pi R_i^2$) can be ignored. Therefore, all laser spots transmitted on the reference plane perpendicular to the normal of the SBCU are reduced to the circles for facilitating the simulation calculation. R_0 and R_i are the spot radii of the two laser beams after a certain transmitting distance (l). The corresponding overlapping area and beam separation distance are expressed as S and d_l, respectively.

According to the geometric relationship of laser transmission, the various formulas of R_0, R_i, and d_l can be obtained separately:

$$R_0 = tan(\theta_c/2) \times l + r_0 \tag{1}$$

$$R_i = tan(\theta_c/2) \times \sqrt{(D - d_l)^2 + l^2} + r_0 \tag{2}$$

$$d_l = D \times |(F - l)/F| \tag{3}$$

where θ_c is the divergence full angle of each beam and after passing through the SBCU. The geometric center of the center beam spot is the coordinate origin, as shown in Fig. 2(b). The equations of the above two circular beam spots and the coordinates (h_l) of their intersections are as follows:

$$x^2 + y^2 = R_0^2 \tag{4}$$

$$(x - d_l)^2 + y^2 = R_i^2 \tag{5}$$

$$h_l = (4R_0^2 + d_l^2 - 4R_i^2)/2d_l \tag{6}$$

The overlapping area (S) and the overlapping efficiency (η) of the above two beam spots can be expressed as:

$$S = 2\left[\int_{h_l}^{R_0} \sqrt{R_0^2 - x^2}dx + \int_{d_l - R_i}^{h_l} \sqrt{R_i^2 - (x - d_l)^2}dx\right]$$
$$= R_i^2\left[\arcsin\left((h_l - d_l)/R_i^2\right) - \arcsin\left(h_l/R_i\right)\right] + \frac{\pi}{2}\left(R_0^2 + R_i^2\right) + (h_l - d_l)\sqrt{R_i^2 - (h_l - d_l)^2} - h_l\sqrt{R_i^2 - h_l^2} \tag{7}$$

$$\eta = S/\left(\pi R_i^2\right) \tag{8}$$

It is not difficult to see from Eq. (1) to Eq. (8) that to obtain the accurate values of η, F, θ_c, the values of D and r_0 should be defined beforehand. In the traditional perforation of the oil well by the perforating bullet, the larger hole-diameter is beneficial to reduce the velocity of the fluid and its ability to carry sand, thereby achieving the purpose of sand control and improved permeability. However, an excessively large hole-diameter will seriously affect the strength of the casing in the oil and gas well. Therefore, conventional oil well perforations are generally recommended to have hole-diameter between 20 mm and 40 mm, and the corresponding maximum perforation depth is about 1 meter [25]. According to this, F was set as 1.2 m, taking into account the diameter of oil well and a safe laser perforation distance. Considering that the diameter of the beam combined laser is varied on both sides of the focal spot, its influence on the hole-diameter is relatively large. The focal spot diameter (C_F) of the SBCU was set as 20 mm ($C_F = 2R_i = 20.0$ mm, when $l = F = 1.2$ m). Under the paraxial approximation ($r_0 \to 0$), the θ_c was calculated as 16.9 mrad based on Eq. (1). When $F = 1.2$ m, $R_i = 10$ mm, $\theta_c = 16.9$ mrad, and $r_0 = 0$, the variations between η and l at different values of D are shown in Fig. 3(a) using Eqs. (1)-(8) and the Matlab software. It is not difficult to find that increasing η and the beam combining length (Δl) is based on the premise of compressing the D as much as possible. However, the 8-mm diameter of each SMA 905 fiber connector places an unfavorable limit on the shortest D. Therefore, on the premise of ensuring that the 19 fiber connectors can be arranged in close concentric circles, the minimum beam separation distance (D_1) between the collimated center beam spot and any other collimated beam spot arranged along the inner ring was set to 12 mm. And the minimum beam separation distance (D_2) between the collimated center beam and any other collimated beam arranged along the outer ring was set to 24 mm.

However, the size of r_0 cannot be ignored in actual design work. Therefore, when $F = 1.2$ m, $R_i = 10$ mm, $\theta_c = 16.9$ mrad, $D_1 = 12$ mm and $D_2 = 24$ mm, Figs. 3(b) and 3(c) show the variations between η and l under different values of r_0. It can be seen that r_0 should be maximized to achieve greater η and Δl. However, there is an upper limit to the maximum value of r_0, which is limited by the minimum value of D and the machining accuracy of the ISBC. When D_1 was 12 mm, the maximum diameter (d_s) of the spherical lens used for each BCU was determined as 10 mm. According to the conventional method, i.e., the maximum ratio between the diameter (d) of the collimated beam and the d_s of the spherical lens is 70%, and d was calculated to be 7.0 mm. To reduce the design error, the size difference between the beam spot on the exit surface of the BCU and the beam spot on the incident surface of the SBCU should be reduced to a minimum. Therefore, the maximum value of r_0 was set to $d/2$ and its value was equal to 3.5 mm, and the corresponding θ_c was revised to 10.8 mrad according to Eq. (1). The initial values ($r_0 = 3.5$ mm, $F = 1.2$ m, $R_i = 10$ mm, $\theta_c = 10.8$ mrad, $D_1 = 12$ mm and $D_2 = 24$ mm)

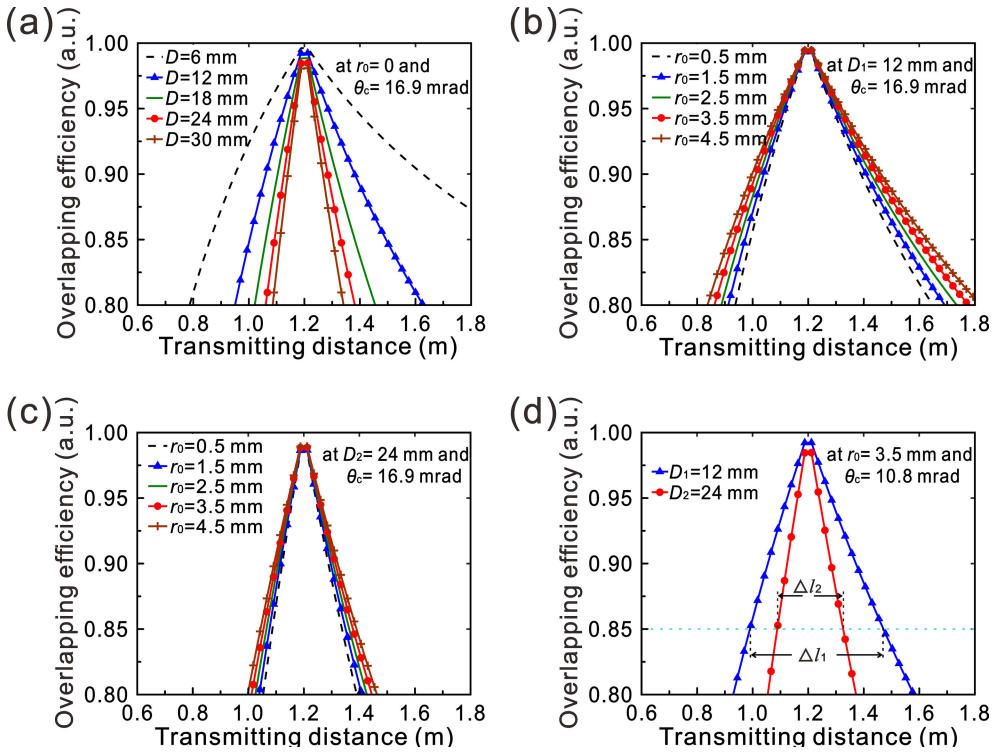

FIGURE 3. Relationships of the overlapping efficiency (η) versus transmitting distance (l) of each laser beam after passing through the SBCU at (a) $r_0 = 0$, $\theta_c = 16.9$ mrad and different D; (b) $D_1 = 12$ mm, $\theta_c = 16.9$ mrad and different r_0; (c) $D_2 = 24$ mm, $\theta_c = 16.9$ mrad and different r_0; (d) $D_1 = 12$ mm, $D_2 = 24$ mm and $\theta_c = 10.8$ mrad.

of the ISBC were finally determined based on the analysis above. The variations between η and l are shown in Fig. 3(d). When $D_1 = 12$ mm and $D_2 = 24$ mm, the beam combining lengths reached 490 mm (Δl_1) and 240 mm (Δl_2), respectively. Obviously, the above results can only estimate that the combined length was in the range of 240 mm to 490 mm, and it was impossible to give a more accurate value of Δl. Therefore, it is necessary to optimally design the parameters of the optical lenses used for the BCU and the SBCU based on the optical parameters obtained above, and to accurately judge the value of Δl by using the cross-sectional energy simulation distributions of the beam combined laser.

The relationships between diameter (d) and divergence full angle (θ) of the collimated beam are shown in empirical Eqs. (9)-(10) based on the Fermat's principle [27]:

$$\theta = \arctan(M_d/f) \tag{9}$$

$$d = M_d + 2f \times \arctan(\theta_0/2) \tag{10}$$

where f is the overall focal length of the BCU. When the 7.0 mm initial set the value of d was substituted into Eqs. (9)-(10), θ and f were calculated as 29.5 mrad and 14.9 mm, respectively.

Based on the initial optical parameters ($M_d = 440\mu$m, $\theta_o = 2\times\arcsin(0.22)$, and $f = 14.9$ mm), a structure model of the BCU has been established by using a Zemax software with the ray-tracing. In order to eliminate chromatic aberration and stray light as much as possible, each collimating unit was composed of three spherical lenses (m_1, m_2, and m_3). The schematic of the BCU is in Fig. 4(a) and 4(c). By optimizing the variables, d and θ of the collimated beam were brought closer to the initial set 7.0 mm and 29.5 mrad, respectively. Finally, the optimized diameter (φ_i, = 1, 2, 3), thickness (z_i), and curvature radii (a_{i1}, a_{i2}) of the two surfaces for spherical lenses m_1, m_2 and m_3 were ($\varphi_1 = 7.0$ mm, $z_1 = 2.0$ mm, $a_{11} = -75.0$ mm, $a_{12} = +5.3$ mm), ($\varphi_2 = 12.0$ mm, $z_2 = 1.5$ mm, $a_{21} = +20.0$ mm, $a_{22} = -11.7$ mm) and ($\varphi_3 = 12.0$ mm, $z_3 = 3.5$ mm, $a_{31} = +30.0$ mm, $a_{32} = +15.7$ mm), respectively. The optimized distances (p_0, p_1, and p_2) between the two adjacent surfaces of the optical components (fiber, m_1, m_2, and m_3) were 5.4 mm, 9.6 mm and 4.1 mm in sequence.

Similarly, the initial optical parameters ($D = 12$ mm and 24 mm, $r_0 = 3.5$ mm, $\theta_c = 10.8$ mrad, and $F = 1.2$ m) were entered into the Zemax software for establishing the structure model of the SBCU. On this basis, this structure model was embedded in the TracePro software to simulate the cross-sectional energy distribution of the beam combined laser. The parameters of the optical lenses used for the SBCU were optimized by comparing different simulation results. The ultimate purpose was to bring the C_F of the SBCU close to the initial setting of 20 mm and obtain a longer Δl. During the simulation, the laser power distribution of each semiconductor laser transmitted in fiber was approximately a Gaussian distribution. As a result, an optimized structure of the SBCU

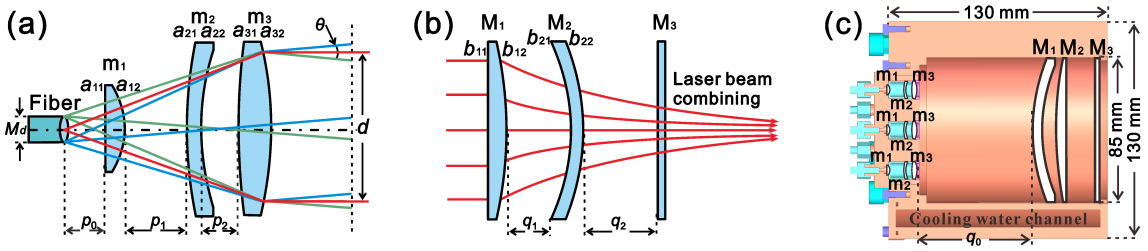

FIGURE 4. Schematics of (a) the BCU, (b) the SBCU, (c) the ISBC.

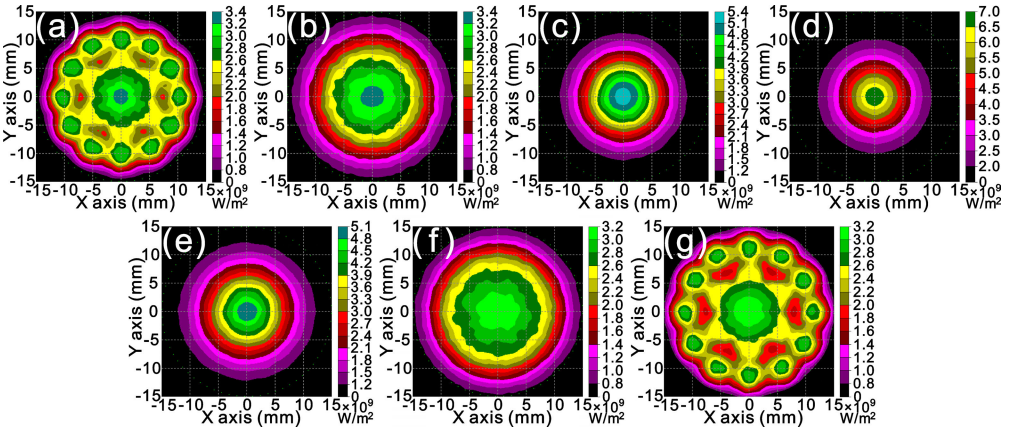

FIGURE 5. Simulated cross-sectional energy simulation distributions of the beam combined laser in the beam combining length, where the focal spot is located at 0 points. The z is the distance between the corresponding cross section and the focal spot. (a) z = −145 mm, (b) z = −140 mm, (c) z = −50 mm, (d) z = 0 mm, (e) z = +50 mm, (f) z = +160 mm, (g) z = +165 mm.

with three spherical lenses (M_1, M_2, and M_3) was determined, as shown in Fig. 4(b) and 4(c). The diameters of M_1, M_2, and M_3 were 85 mm, which was equivalent to the optical aperture of the space beam combiner. The thickness (Z_i) and curvature radii (b_{i1}, b_{i2}) of two surfaces for spherical lenses M_1 and M_2 were ($Z_1 = 8.0$ mm, $b_{11} = +\infty$, $b_{12} = +510$ mm) and ($Z_2 = 10.0$ mm, $b_{21} = -105.0$ mm, $b_{22} = +110.0$ mm), respectively. M_3 was a plane lens with a thickness of 3 mm to prevent the SBCU from being contaminated. The optimized distances (q_0, q_1, and q_2) between the two adjacent surfaces of the optical components (m_3, M_1, M_2, and M_3) were 65.0 mm, 22.0 mm and 28.0 mm in sequence.

When the output power of each semiconductor laser was 550 W, the simulated cross-sectional energy distributions of the beam combined laser at different positions were obtained by using the TracePro, as shown in Figs. 5(a)-5(g). Along the direction of laser propagation, i.e. in the order from Fig. 5(a) to Fig. 5(g), the relative distances between the laser spot described in each diagram and the focal spot of the beam combined laser were −145 mm, −140 mm, −50 mm, 0 mm, +50 mm, +160 mm and +165 mm, respectively. Figure 5(d) shows the simulated energy distribution of a combined focal spot with a diameter approaching the initial value of 20 mm. As can be seen from Fig. 5(b) to Fig. 5(f), the cross-sectional energy distributions of the beam combined laser are similar to the cross-sectional energy distribution of a single Gaussian laser beam. The relative distance between Fig. 5(b) to Fig. 5(f) is 300 mm. The relative distance between Fig. 5(a) and Fig. 5(b) and the distance between Fig. 5(g) and Fig. 5(f) are only 5 mm. The beam combining length Δl was determined to be 300 mm, which is a judgment that the cross-sectional energies distributions of the combined beams shown in Fig. 5(a) and Fig. 5(g) both exhibit discrete characteristics. It also shows that the Δl is the result of the interaction of Δl_1 and Δl_2.

III. EXPERIMENTAL SETUP

According to the optimized optical parameters of the BCUs and SBCU by numerical simulations, a water-cooled 19 × 1 ISBC with brass as processing material was developed as shown in the inset in Fig. 6. Considering the requirement of adequate heat dissipation for stable operation of the 19 × 1 ISBC, the cylindrical space with a diameter of 85 mm formed by the BCUs and SBCU was enclosed by an annular cooling water jacket. The diameter of the cooling water passage inside the jacket was designed to be 10.5 mm to ensure water flow rate larger than 4.0 L/min, water pressure less than 0.5 MPa and water temperature at 20°C (these are consistent with the cooling water system parameters required by the 19 semiconductor lasers). This was advantageous for rapidly removing ∼ 1 kW of heat generated by the optical loss. In order to counteract the adverse effects of stress deformation during

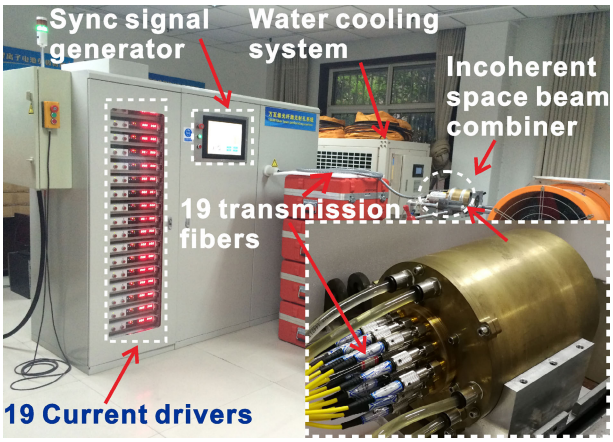

FIGURE 6. Photo of incoherent space laser beam combining system. The inset is a photo of the combiner.

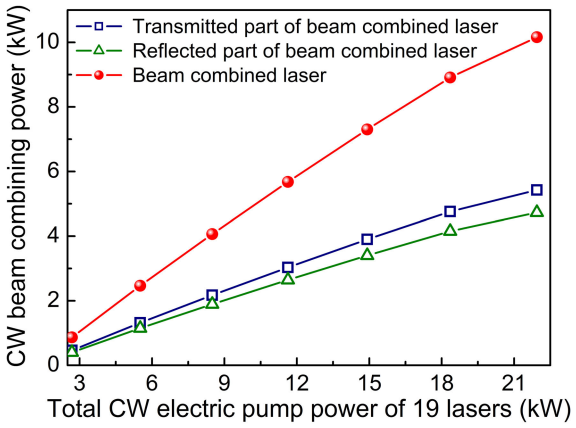

FIGURE 7. CW power of the beam combined laser as a function of total electric pump power of the 19 semiconductor lasers.

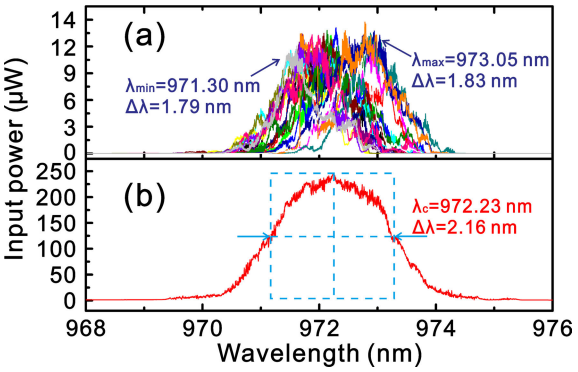

FIGURE 8. (a) Spectral superposition from 19 semiconductor lasers running separately, and (b) spectrum of the beam combined laser.

machining on the overall structural strength of the combiner, the inner and the outer wall thicknesses of the jacket were determined to be 6 mm, respectively. The outer diameter of the combiner was determined to be 130 mm according to the structural parameters above. The smaller external diameter ensures that the space beam combiner can be placed in most oil wells. Of course, the outer diameter of the combiner will be further reduced by optimizing the structural parameters.

In order to ensure that 19 collimated laser beams were parallel to each other, the 19 BCUs and a SBCU were integrally machined, and the precision of machining was also set to a high standard. For example, the coaxiality of the fiber end faces, m_1, m_2, and m_3 spherical lenses in each BCU should be less than 0.02 mm. The verticality between the normal of each fiber end face and the same mechanical cross section of the combiner (laser incident plane) should be less than 1 mrad. After the beam combiner was machined, a high precision laser auto-collimation theodolite was used to measure the coaxiality and verticality of each BCU. The each measured coaxiality was less than 0.016 mm, and the each verticality was less than 0.65 mrad.

The both surfaces of all the optical lenses were coated for anti-reflection ($R < 0.4\%$) at 972 nm. Then, a fiber-transmission incoherent space laser beam combining system was developed using 19 semiconductor lasers a wavelength of 972 nm, as shown in Fig. 6. Every semiconductor laser was cooled with water and controlled by an independent current driver. A sync signal generator was used to precisely synchronously control the driving currents of the independent current drivers.

In the experiment, a splitter lens with a transmittance of 53.42% and a reflectance of 46.58% at 972 nm was used to measure the CW beam combining power. Under the synchronous operation of 19 semiconductor lasers, a maximum CW beam combining power of 10.159 kW was obtained, corresponding to a 10.341 kW maximum total output power and a 21.95 kW maximum total electric pump power of the 19 semiconductor lasers. Among them, the transmitted and reflected powers of the combined beam were 5.427 kW and 4.732 kW, respectively, as shown in Fig. 7. The beam combining efficiency and electro-optic conversion efficiency of the space beam combining were 98.24% and 46.28%, respectively.

In 20 minutes, the CW power was measured in 3 seconds time step. The power instability of the beam combined laser beam was calculated as ±1.2%. The center wavelengths of 19 semiconductor lasers from 971.30 nm to 973.05 nm was measured experimentally, corresponding to the line widths ranging from 1.79 nm to 1.83 nm, respectively, as shown in Fig. 8(a). Figure 8(b) illustrates the measured spectrum of the synchronously operated combination beam, which gives a central wavelength of 972.23 nm and a linewidth of 2.16 nm. The results show that the incoherent space beam combination remains the narrow linewidth.

In addition, a steel plate with a thickness of 2 mm was used as a marking plate within 500 ms to mark the true cross-sectional profile of the 10 kW beam combined laser, as shown in Fig. 9. Comparing Figs. 9(a)-(i) with Figs. 5(a)-(i) at the same position, the higher level of consistency between the diameters of the simulated beam combined laser and the diameters of the real beam combined laser are demonstrated.

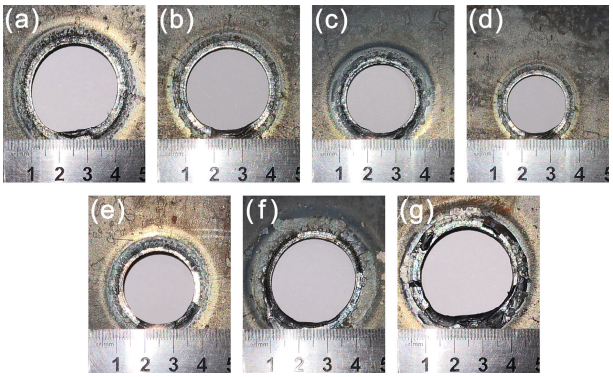

FIGURE 9. The measured cross-sectional shape of the of the beam combined laser in the beam combining length, where its focal spot is located at 0 point. The z is the distance between the corresponding cross section and the focal spot. (a) z = −145 mm, (b) z = −140 mm, (c) z = −50 mm, (d) z = 0 mm, (e) z = +50 mm, (f) z = +160 mm, (g) z = +165 mm.

And the space beam combined laser beam has excellent overlap over a beam combining length of 300 mm. The measured diameter of the combined focal spot was about 21 mm, as shown in Fig. 9(d). At the left and right edges of the beam combining length, the diameters of the corresponding two profiles were about 30 mm. These comparisons show that our simulation work is in good accuracy.

IV. LASER PERFORATION

The analysis of the temperature distribution on the surface and inside the rock by heat conduction equation is an effective tool to judge whether the above beam combined laser with 10 kW can be applied to the laser perforation or not. A granite sample with a SiO_2 content of about 70% was first used to simulate laser perforation [28]. Its length is 960 mm and section size is 200 mm × 140 mm. The temperature field distribution of the rock by Gaussian laser irradiating for t seconds can be given by [29]:

$$T(x,y,z,t) - T_0 = \frac{2\alpha_0 P_0 \sqrt{\rho G_r}}{k\pi^{3/2}} \times \int_0^t \frac{\exp\left[\frac{-2(x^2+y^2)}{8\rho G_r(t-\tau)+R_L^2} - \frac{z^2}{4\rho G_r(t-\tau)}\right]}{\sqrt{t-\tau}\left[8\rho G_r(t-\tau)+R_L^2\right]} d\tau \quad (11)$$

where T(x, y, z, t) is the temperature field of the rock under laser irradiation, T_0 is room temperature and it is set to 27°C; P_0 and R_L are the power and waist radius of the beam combined laser, respectively; t is the laser irradiation time, τ is the time integral variables; ρ, k, and G_r is the measured density, thermal conductivity and specific heat of the granite, respectively; α_0 is the surface absorption coefficient of the granite for near-infrared laser at normal incidence and it is usually set to 90%; x-axis and y-axis constitute the plane surface of the rock, and z-axis is the direction of laser propagation.

Under room temperature and atmospheric pressure, measured ρ, k, and $G_r$are 2.71 × 10^3 kg/m^3, 3.02 W/(m·°C), and 0.95 × 10^3 J/(kg·°C), respectively. The t, P_0, and R_L are sequentially set to 1 second, 10 kW, and 10.5 mm substituted into the Eq. (11), the 3D and (b) 2D temperature field distribution on the surface of the granite sample ($z = 0$) are shown in Fig. 10(a) and 10(b), respectively. And the temperature field distribution inside the granite sample ($y = 0$) is shown in Figs. 10(c). In a conical region with a bottom diameter of 21 mm and a depth of 6.8 mm, the temperature exceeds the 1650 °C-melting point of the granite. The simulation results show that the beam combined laser can complete the laser perforation task under very short irradiation time and limit the beam combining power. The calculated laser perforation speed is 6.8 mm/s.

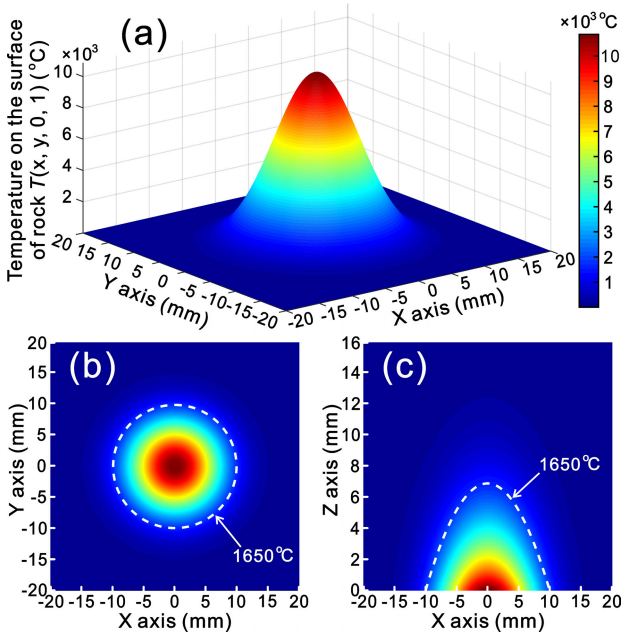

FIGURE 10. (a) 3D and (b) 2D temperature field distribution on the surface of granite sample, (c) temperature field distribution inside the granite sample after 10 kW beam combined laser irradiating for 1 s.

As a verification of the simulation results, a 10 kW beam combined laser was used to perform the laser perforation experiment on the granite sample. The experimental site of laser perforation is shown in Fig. 11(a). While the laser illuminates the granite sample, the ISBC moved slowly horizontally toward the granite sample. The part of rock irradiated was rapidly melted under 10 kW laser irradiating. As shown in Fig. 11(b), a rock hole with a large amount of glazed material was formed. For granite, thermal crushing and thermal melting caused by absorbing high power density light are the main reasons to break and melt the rock. When the total amount of time for laser irradiation t reached 325 s, the granite sample with a length of 960 mm was penetrated by the 10 kW beam combined laser, and the corresponding laser perforation velocity was about 2.95 mm/s, as shown in Fig. 11(e). This indicates that the experimentally obtained space beam laser possesses a higher cross-sectional power density due to its smaller spot size, excellent overlap

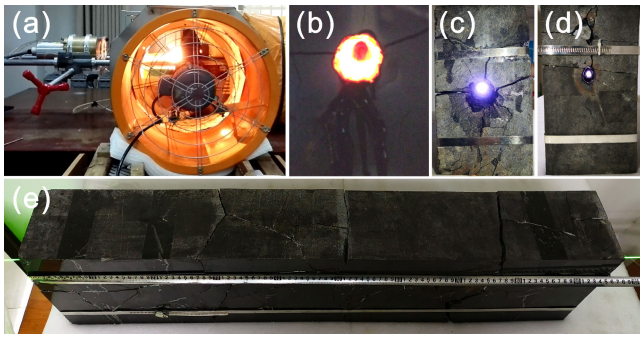

FIGURE 11. Photos of (a) the scene and (b) the rock hole of the laser perforation experiment. Photos of (c) the laser incident cross section, (d) the laser ejection cross-section, and (e) a standard granite sample drilled. A green fluorescent fiber is used to show that the granite sample is shot through.

and longer beam combining length. This was the key to obtaining a laser perforation length of 960 mm. As shown in Figs. 11(b)-11(e), a large number of obvious micro-cracks appeared around the perforation tunnel in the granite sample. This will help to enhance permeability and recovery of the oil and gas. However, a large amount of dust and molten matter in the rock pores not only scatters a large amount of laser energy, but also transfers part of the absorbed laser energy to the non-irradiated area in the form of heat [30]. As a result, the laser power was forced to be greatly attenuated while the laser perforation speed was also limited to a low level of 2.95 mm/s. Further increasing the laser power will be an effective choice for increasing the laser perforation rate. One of the advantages of our incoherent spatial beam combiner is that up to 19 fiber-transmitted semiconductor laser beams are used for laser incoherent space beam combining, which effectively reduces the transmission power and transmission risk of the sum lasers in a single fiber. Therefore, we can significantly increase the beam combining power to meet the requirements for oil well laser perforation by properly increasing the power of each semiconductor laser.

V. CONCLUSION

In conclusion, we have successfully demonstrated a 972 nm incoherent space beam combined laser with a maximum CW beam combining power of 10.159 kW by using a proprietary 19×1 ISBC. The beam combining efficiency is up to 98.2%, resulting in a beam combining length of 300 mm, a focal spot diameter of 21 mm and a line width of 2.16 nm. Besides, we also performed a successful laser perforation experiment in a granite sample using a 10 kW space beam combined laser and obtained a perforation length of 960 mm. The 130 mm of external diameter ensures that our ISBC can be placed in most oil wells. Up to 19 fiber-transmitted laser beams for laser combination can effectively disperse the laser power for oil well laser perforation, thereby, improving the safety of ultra-high power laser transmission in oil wells. Compared with other incoherent combining devices such as all-fiber combiner and spectral beam combining grating, our incoherent space beam combiner based on traditional optical design, manufacture and debugging technology has the advantages of multi-channel plug-and-play, low price (<$10,000), high yield, and high structural strength. Therefore, it will be a very promising incoherent combiner in ultrahigh power laser applications such as oil well laser perforation, laser quenching, laser welding and laser cladding.

REFERENCES

[1] Z. Xu, C. B. Reed, G. Konercki, R. A. Parker, B. C. Gahan, S. Batarseh, and N. Skinner, "Specific energy for pulsed laser rock drilling," *J. Laser Appl.*, vol. 15, no. 1, pp. 25–30, Feb. 2003.

[2] K. R. Agha, H. A. Belhaj, S. Mustafiz, N. A. Bjorndalen, and M. R. Islam, "Numerical investigation of the prospects of high energy laser in drilling oil and gas wells," *Petrol. Sci. Technol.*, vol. 22, no. 9, pp. 1173–1186, Jan. 2004.

[3] Z. Y. Xu, Y. Yamashita, and C. Reed, "Modeling of laser spallation drilling of rocks for gas-and oil well drilling," in *Proc. Tech. Conf. Exhib.*, 2005, Art. no. 95746-MS.

[4] B. M. Olaleye, "A review of light amplification by stimulated emission of radiation in oil and gas well drilling," *Mining Sci. Technol.*, vol. 20, no. 5, pp. 752–757, Sep. 2010.

[5] R. Keshavarzi, R. Jahanbakhshi, H. Bayesteh, A. Ghorbani, and M. A. Shoorehdeli, "Applying high power lasers in perforating oil and gas wells: Prediction of the laser power loss during laser beam-fluid interaction by using artificial neural networks," *Lasers Eng.*, vol. 21, nos. 5–6, pp. 329–340, Oct. 2011.

[6] H. Kariminezhad, H. Amani, and M. Moosapoor, "A laboratory study about laser perforation of concrete for application in oil and gas wells," *J. Nat. Gas Sci. Eng.*, vol. 32, pp. 566–573, May 2016.

[7] M. R. Erfan, K. Shahriar, M. Sharifzadeh, M. Ahmadic, and M. J. Torkamany, "Moving perforation of rocks using long pulse Nd:YAG laser," *Opt. Lasers Eng.*, vol. 94, pp. 12–16, Jul. 2017.

[8] J. W. Dawson, M. J. Messerly, R. J. Beach, M. Y. Shverdin, E. A. Stappaerts, A. K. Sridharan, P. H. Pax, J. E. Hseebner, C. W. Siders, and C. P. J. Barty, "Analysis of the scalability of diffraction-limited fiber lasers and amplifiers to high average power," *Opt. Express*, vol. 16, no. 17, pp. 13240–13266, Aug. 2008.

[9] A. V. Smith and J. J. Smith, "Mode instability in high power fiber amplifiers," *Opt. Express*, vol. 19, no. 11, pp. 10180–10192, May 2011.

[10] A. V. Smith and J. J. Smith, "Influence of pump and seed modulation on the mode instability thresholds of fiber amplifiers," *Opt. Express*, vol. 20, no. 22, pp. 24545–24558, Oct. 2012.

[11] C. M. Lei, Y. Gu, Z. Chen, Z. Wang, P. Zhou, Y. Ma, H. Xiao, J. Leng, X. Wang, J. Hou, X. Xu, J. Chen, and Z. Liu, "Incoherent beam combining of fiber lasers by an all-fiber 7×1 signal combiner at a power level of 14 kW," *Opt. Express*, vol. 26, no. 8, pp. 10421–10427, Apr. 2018.

[12] X. Zhou, Z. Chen, Z. Wang, J. Hou, and X. Xu, "Beam quality analysis of incoherent beam combining by a 7×1all-fiber signal combiner," *IEEE Photon. Technol. Lett.*, vol. 28, no. 20, pp. 2265–2268, Oct. 15, 2016.

[13] D. Noordegraaf, M. D. Maack, P. M. W. Skovgaard, J. Johansen, F. Becker, S. Belke, M. Blomqvist, and J. Laegsgaard, "All-fiber 7×1 signal combiner for incoherent laser beam combining," *Proc. SPIE*, vol. 7914, Feb. 2011, Art. no. 79142L.

[14] F. Chen, J. Ma, C. Wei, R. Zhu, W. Zhou, Q. Yuan, S. Pan, J. Y. Zhang, Y. Wen, and J. Dou, "10 kW-level spectral beam combination of two high power broad-linewidth fiber lasers by means of edge filters," *Opt. Express*, vol. 25, no. 26, pp. 32783–32791, Dec. 2017.

[15] Y. Zheng, Y. Yang, J. Wang, M. Hu, G. Liu, X. Zhao, X. Chen, K. Liu, C. Zhao, B. He, and J. Zhou, "10.8 kW spectral beam combination of eight all-fiber superfluorescent sources and their dispersion compensation," *Opt. Express*, vol. 24, no. 11, pp. 12063–12071, May 2016.

[16] C. Wirth, O. Schmidt, I. Tsybin, T. Schreiber, R. Eberhardt, J. Limpert, A. Tünnermann, K. Ludewigt, M. Gowin, E. T. Have, and M. Jung, "High average power spectral beam combining of four fiber amplifiers to 8.2 kW," *Opt. Lett.*, vol. 36, no. 16, pp. 3118–3120, Aug. 2011.

[17] R. Protz, J. Zoz, F. Geidek, S. Dietrich, and M. Fall, "High-power beam combining: A step to a future laser weapon system," *Proc. SPIE*, vol. 8547, Nov. 2012, Art. no. 854708.

[18] P. Sprangle, A. Ting, J. Penano, R. Fischer, and B. Hafizi, "Incoherent combining and atmospheric propagation of high-power fiber lasers for directed-energy applications," *IEEE J. Quantum Electron.*, vol. 45, no. 2, pp. 138–148, Feb. 2009.
[19] C. Wirth, O. Schmidt, I. Tsybin, T. Schreiber, T. Peschel, F. Brückner, T. Clausnitzer, J. Limpert, R. Eberhardt, A. Tünnermann, M. Gowin, E. T. Have, K. Ludewigt, and M. Jung, "2 kW incoherent beam combining of four narrow-linewidth photonic crystal fiber amplifiers," *Opt. Express*, vol. 17, no. 3, pp. 1178–1183, Feb. 2009.
[20] Y. Y. Jin, Y. Zou, X. Ma, J. Li, Y. Li, L. Jin, L. Xu, W. Zhao, Q. Sui, and Z. Zhang, "Study on laser diode incoherent beam combining technology based on tracepro," in *Proc. IEEE Int. Conf. OptoElectron. Microelectron.*, Aug. 2012, pp. 87–90.
[21] M. Shtaif, Y. Shamir, and Y. Sintov, "Beam quality analysis and optimization in an adiabatic low mode tapered fiber beam combiner," *J. Opt. Soc. Amer. B, Opt. Phys.*, vol. 27, no. 12, pp. 2669–2676, 2010.
[22] E. C. Cheung, J. G. Ho, T. S. McComb, and S. Palese, "High density spectral beam combination with spatial chirp precompensation," *Opt. Express*, vol. 19, no. 21, pp. 20984–20990, 2011.
[23] F. Tian, H. Yan, L. Chen, Y. Ye, J. Li, J. Luo, and F. Lu, "Investigation on the influence of spectral linewidth broadening on beam quality in spectral beam combination," *Proc. SPIE*, vol. 9255, Feb. 2015, Art. no. 92553N.
[24] K. Ludewigt, T. Riesbeck, B. Schünemann, A. Graf, M. Jung, T. Schreiber, R. A. Eberhardt, and A. Tünnermann, "Overview of the laser activities at Rheinmetall Waffe munition," *Proc. SPIE*, vol. 8547, Nov. 2012, Art. no. 854704.
[25] Y. Noorollahi, M. Pourarshad, S. Jalilinasrabady, and H. Yousefi, "Numerical simulation of power production from abandoned oil wells in Ahwaz oil field in southern iran," *Geothermics*, vol. 55, pp. 16–23, May 2015.
[26] S. Gharibi, E. Mortezazadeh, S. J. H. A. Bodi, and A. Vatani, "Feasibility study of geothermal heat extraction from abandoned oil wells using a U-tube heat exchanger," *Energy*, vol. 155, pp. 554–567, Jun. 2018.
[27] E. M. Drège, N. G. Skinner, and D. M. Byrne, "Analytical far-field divergence angle of a truncated Gaussian beam," *Appl. Opt.*, vol. 39, no. 27, pp. 4918–4925, 2000.
[28] J. L. Zhang and X. Zhan, "Composition and provenance of sandstones and siltstones in paleogene, huimin depression, bohai bay basin, eastern china," *J. China Univ. Geosci.*, vol. 19, no. 3, pp. 252–270, Jun. 2008.
[29] M. X. Hu, Y. Bai, H. W. Chen, B. Lu, and J. Bai, "Engineering characteristics of laser perforation with a high power fiber laser in oil and gas wells," *Infr. Phys. Techn.*, vol. 92, pp. 103–108, Aug. 2018.
[30] R. Keshavarzi, "Application of high power lasers in perforation and fracture initiation of oil and gas wells," *Laser. Eng.*, vol. 21, no. 3, pp. 149–167, Jan. 2011.

YANG BAI was born in Hanzhong, Shannxi, China, in 1977. He received the B.S. degree from the Department of physics, Northwest University, in 2001, and the Ph.D. degree from the Institute of Photonics & Photon-Technology, Northwest University, in 2010. In 2004, he joined the Northwest University as a Lecturer, where he is currently an Associate Professor. His research interests include high-power, high-energy, narrow-pulse-width all-solid-state lasers, fiber lasers, laser nonlinear frequency variations, optical parametric oscillations, laser combining, and laser perforation.

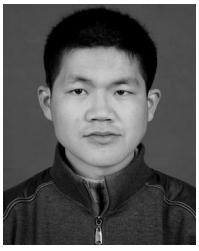

GUANGZHI LEI was born in Yulin, Shannxi, China, in 1978. He received the B.S. degree from the Department of physics, Xi'an Shiyou University, in 2001, and the Ph.D. degree from the Institute of Photonics & Photon-Technology, Northwest University, in 2008. In 2008, he joined the Northwest University as a Lecturer, where he is currently an Associate Researcher. His research interests include fiber lasers, laser nonlinear frequency variations, and laser perforation.

HAOWEI CHEN was born in Yulin, Shannxi, China, in 1978. He received the B.S. degree from the Department of physics, Xi'an Shiyou University, in 2001, and the Ph.D. degree from the Institute of Photonics & Photon-Technology, Northwest University, in 2008. In 2008, he joined the Northwest University as a Lecturer, where he is currently an Associate Researcher. His research interests include fiber lasers, laser nonlinear frequency variations, and laser perforation.

XIAOQIANG FENG was born in Baoji, Shannxi, China, in 1974. He received the B.S. degree from the Department of physics, Northwest University, in 1998, and the Ph.D. degree from the Xi'an Institute of Optics and Precision Mechanics of CAS, in 2004. In 2004, he joined the Northwest University as a Lecturer, where he is currently an Associate Professor. His research interests include the design and development of optical instruments, and opto-mechanical systems.

DIAO LI was born in Xi'an, Shaanxi, China, in 1988. He received the B.S. degree from the Department of Physics and the Ph.D. degree from the Institute of Photonics and Photon-Technology, Northwest University, in 2011, and 2018, respectively. His research interests include low dimensional nanomaterials based ultrafast photonics, fiber laser, and nonlinear optics, including carbon nanotubes, graphene, and related layered materials.

JINTAO BAI was born in Suide, Shannxi, China, in 1959. He received the B.S. degree from the Department of physics, Northwest University, in 1983, and the Ph.D. degree from the Xi'an Institute of Optics and Precision Mechanics of CAS, in 2000. In 2000, he joined the Northwest University as a Professor. His research interests include high-power, high-energy, narrow-pulse-width all-solid-state lasers, fiber lasers, laser nonlinear frequency variations, transient optical, and laser perforation.